International Journal of Greenhouse Gas Control

journal homepage: www.elsevier.com/locate/ijggc

Review and implications of relative permeability of CO_2/brine systems and residual trapping of CO_2

N.M. Burnside *, M. Naylor

Scottish Carbon Capture and Storage, School of Geosciences, University of Edinburgh, EH9 3JW, United Kingdom

ARTICLE INFO

ABSTRACT

The adoption of carbon capture and storage (CCS) as a method of mitigating anthropogenic CO_2 emissions will depend on the ability of initial geological storage projects to demonstrate secure containment of injected CO_2. Potential leakage pathways, such as faults or degraded wells, increase the uncertainty of geological storage security. CCS as an industry is still in its infancy and until we have experience of industrial scale, long term CO_2 storage projects, quantifying leakage event probabilities will be problematic. Laboratory measurements of residual saturation trapping, the immobilisation of isolated micro-bubbles of CO_2 in reservoir pores, provides an evidence base to determine the fraction of injected CO_2 that will remain trapped in the reservoir, even if a leakage event were to occur. Experimental results for sandstone, the most common target lithology for storage projects, demonstrate that 13–92% of injected CO_2 can be residually trapped. Mineralisation, the only other geological trapping mechanism which guarantees permanent trapping of CO_2, immobilises CO_2 over hundreds to thousands of years. In comparison, residual trapping occurs over years to decades, a timescale which is more relevant to CCS projects during their operational phase and to any financial security mechanisms they require to secure storage permits.

© 2014 The Authors. Published by Elsevier Ltd. Open access under the CC BY-NC-ND license.

1. Introduction

Carbon capture and storage (CCS) is a technology that will have to be implemented on a large scale if efforts to decarbonise energy production and industrial processes are to be realised. However, for CCS to be a realistic option for anthropogenic CO_2 emission reduction, geological storage of CO_2 must prove to be robust. Potential leakage pathways, including faults, compromised caprocks and degraded wells have been discussed extensively elsewhere (Burnside et al., 2013). In this paper we focus on geological trapping mechanisms, which can guarantee immobilisation of CO_2 in the reservoir, even in the event of leakage.

Evidence-based estimates of CO_2 trapping need to consider the most important mechanisms for permanent immobilisation of injected CO_2. There are four recognised methods for geological trapping of CO_2 (IPCC, 2005).

(i) Stratigraphic and structural trapping impedes the migration of buoyant CO_2 via high capillary entry pressure barriers created by low permeability formations and geological structures. This mechanism defines the geometry of the store within which more permanent storage can occur but it does not immobilise CO_2 itself.

(ii) Solubility trapping occurs when CO_2 dissolves into the formation brine. CO_2 saturated brine will typically sink as it is denser than the formation brine therefore this mechanism could potentially be important for storage security. However, aqueous CO_2 can still migrate due to ground water flow and any drop in pressure can lead to the liberation of CO_2.

(iii) Mineralisation can trap minimal fractions of injected CO_2 (Baines and Worden, 2004; Wilkinson et al., 2009; Pickup et al., 2010). Mineral trapping is a long term process and may need 10,000s of years to prove to be an effective trapping solution (IPCC, 2005), too long a timescale to have a bearing on storage security over the operational period of storage projects.

(iv) Residual trapping is far more rapid, occurring over time scales of days to months in core scale experiments (Pentland et al., 2011a; Shi et al., 2011a,b), and is predicted to contribute significantly to trapping within 10's of years (Saadatpoor et al., 2010; Sifuentes et al., 2009). Understanding the evidence base for residual saturation trapping can therefore provide a conservative estimate of CO_2 storage security over timescales in line with storage projects.

* Corresponding author at: University of Edinburgh, Department of Geosciences, Grant Institute, Kings Buildings, West Mains Road, Edinburgh EH9 3JW, United Kingdom. Tel.: +44 0131 650 4918; fax: +44 0131 668 3184.

E-mail address: neil.m.burnside@gmail.com (N.M. Burnside).

In this paper we detail the science of residual trapping and analyse a compilation of published experimental results. In particular we explore the role of relative permeability (the ease of CO_2 flow through brine saturated rock) and residual gas saturation (the fraction of CO_2 ultimately trapped within the pore space) as these processes control the volume of injected CO_2 that can become immobilised through residual gas trapping.

We also compare experimental data with values used in CO_2 injection simulations, calculate the effects of incomplete gas saturation; consider the implications of the distribution of experimental results on injectivity and discuss the application of experimental data to the insurability of geological storage reservoirs.

The availability of published residual saturation data is currently sparse due to the expensive and time consuming nature of laboratory experiments, and confidentiality issues around specific storage sites. Nonetheless, available data provides the foundation of an evidence base, particularly for typical reservoir quality sandstones, that can be used to quantify the volume of injected CO_2 that will remain securely stored; even if the storage site is compromised.

2. Estimating and measuring relative permeability and residual saturation

Residual trapping is controlled by a range of physical and chemical factors including rock pore network geometry, rock–fluid interactions and fluid–fluid interactions. Rock specific properties are summarised through various empirical metrics including permeability, porosity, gas relative permeability; gas saturation, wettability and capillary entry pressure (Juanes et al., 2006; Nghiem et al., 2009).

Effective porosity is the fraction of the rock pore space accessible to fluid phases. Intrinsic (or absolute) permeability, a factor independent of fluid properties, describes a rock's ability to permit fluid flow through its effective porosity; with the size of pore throats, degree of pore interconnection and volume of open space all playing a significant role (Fetter, 1993). Effective permeability describes conductance of a fluid though a pore space network that is already partially saturated with an immiscible fluid. Measurement of this parameter is important for determining the flow rate of oil through the pore space of a producing reservoir in the presence of formation brine (Anand et al., 2010).

Wettability, the contact angle of saturating fluids with rock, has a key influence over fluid permeabilities within the pore space (Spiteri et al., 2008). If the fluid–rock contact angle is <90° then the pore surface is preferentially covered by that fluid and it becomes known as the 'wetting fluid'. Under typical reservoir conditions the rock will be brine wet and injected CO_2, with a contact angle of >90°, will act as a 'non-wetting fluid'.

For multiphase flow, the relative permeability (k_r) is the ratio of the effective permeability of a particular fluid, at a given saturation, to the intrinsic permeability of the rock. Saturation describes the proportion of the pore space volume that is occupied by a particular fluid. Relative permeability provides an empirical description of the reduction in fluid flow due to surface-tension effects between fluids; and chemical interaction between fluids and the mineralogy of the rock matrix. In this paper we use the term $k_r^{CO_2}$ to describe the end point relative permeability of CO_2 at maximum CO_2 saturation (S_{max}).

Where CO_2 and brine are both present within a pore network, we can attempt to flush CO_2 from the pores using the brine. However, it is not possible to drive all of the CO_2 out since a fraction of it will become disconnected and immobile. The proportion of pore space filled with this remaining CO_2 is described as trapped saturation (S_t). At this point k_r has dropped to zero reflecting the fact that the fluid no longer flows out of the rock (Fig. 1). Note that determining
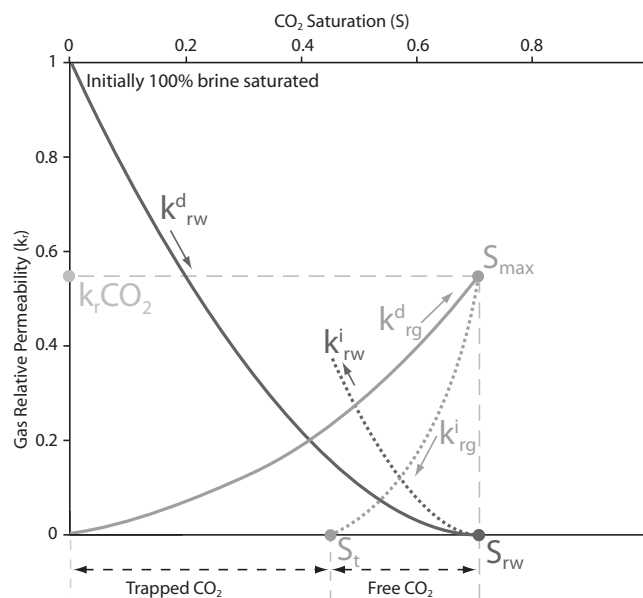

Fig. 1. An example of a typical relative permeability curves for drainage and imbibition recorded throughout experimentation. At the start of the experiment rock core samples are fully saturated with brine. During the drainage phase CO_2 saturation increases and the gas relative permeability follows the grey drainage curve (k_{rg}^d) whilst brine saturation drops along the dark grey drainage curve (k_{rw}^d) as brine is displaced from the core. End point maximum gas saturation (S_{max}) is obtained when brine relative permeability equals zero and brine residual saturation (S_{rw}) is reached. At this stage endpoint CO_2 relative permeability ($k_r^{CO_2}$) is reached. Brine is then injected back into the core sample, if it is able to re-occupy the pore space CO_2 saturation decreases along the dashed grey imbibition curve (k_{rg}^i) and brine saturation starts to recover, dark grey dashed curve (k_{rw}^i). When CO_2 permeability drops to zero no more CO_2 can be displaced from the pore space of the sample and the residual or trapped gas saturation (S_t) is reached.

$k_r^{CO_2}$ is not necessary for measuring S_t, though it is important for calculating evolving flow rates and injectivity.

A number of labs have performed experiments on core samples 10–100 mm in scale to measure end point $k_r^{CO_2}$, S_{max} and S_t for CO_2–brine systems under reservoir conditions (typical pressures and temperatures of 35–70 °C and 9–27 MPa; Table SM1). The results are dependent upon rock sample, brine composition, thermodynamic regime and experimental setup. By convention, drainage (k_{rg}^d) is defined as CO_2 injection into a brine saturated rock until S_{max} is achieved, and imbibition (k_{rg}^i) is defined as the process after flow reversal where brine flushes back through rock that has some level of CO_2 saturation until k_r drops to zero and S_t is reached (Fig. 1).

Supplementary material related to this article can be found, in the online version, at doi:10.1016/j.ijggc.2014.01.013.

Physically, imbibition traps CO_2 within the rock pore-space via two separate hysteresis effects which are controlled by the pore space saturation history, the phase relative permeabilities and the capillary pressures of the saturation path (Spiteri et al., 2008). Contact angle hysteresis occurs when chemical heterogeneities or surface roughness leads to the advancing brine having higher angle of contact in comparison to the receding CO_2 (Juanes et al., 2006). Snap-off of disconnected CO_2 droplets occurs when ganglions of CO_2 become isolated from the plume by encroaching brine. At the reservoir scale these hysteresis effects occur when brine encroaches into the tail of relatively buoyant CO_2 plumes as they migrate through the storage reservoir.

Importantly, the ratio of S_t to S_{max} gives the fraction of CO_2 that is immobilised in the sample, if S_{max} is reached during drainage. The trapping ratio (R) value represents the quantifiable proportion of the CO_2 present within a storage reservoir that will always remain

trapped within the pore space of the rock. As we will show in Section 4.2, theory suggests that the trapping ratio is greater than R when the maximum saturation obtained during drainage is less than S_{max}, thus use of R in estimating the proportion of secure CO_2 is conservative.

2.1. Experimental procedures for relative permeability and residual saturation endpoint measurements

In this section we describe typical experimental procedures behind measuring end point $k_r^{CO_2}$, S_{max} and S_t, and discuss how experimental design can bias measurements and hence bias the trapped proportion (R). The majority of experiments have solely focused on drainage and finding $k_r^{CO_2}$ values for CO_2 injection; in part because imbibition adds complexity, time and cost to experiments. Experiments are typically carried out on 30–200 mm scale rock cores (for schematics of typical set-ups see Bennion and Bachu, 2008; Shi et al., 2011a). The wetting phase typically constitutes brine from the sample location, in order to minimise chemical modifications, and the pressure cell allows replication of reservoir pressure and temperature conditions. Depending upon the experimental design, there are a range of limitations which can add a degree of uncertainty to experimental results (Perrin and Benson, 2010). Issues with low flow rates and doping of brine to better track fluid fronts are discussed below and there is the overlying issue that the way the experiment is conducted may not coincide with the orientation of actual flow directions in the storage reservoir (Crotti et al., 1998).

The typical experimental workflow starts by measuring absolute permeability. Air is removed from the pore space of the core by either using a vacuum pump (Bennion and Bachu, 2005) or injecting CO_2 at a low flow rate in ambient conditions for a period of 12 h (Perrin and Benson, 2010) and then saturating with gas-free formation water. If CO_2 has been used to evacuate pore space the majority of it is displaced by or dissolved into the brine (Perrin and Benson, 2010). The ideal scenario is 100% water saturation; however this is difficult to achieve. Shi et al. (2011a,b) note residual air (3.5–4.2% saturation) in core samples after brine saturation and suggest this is likely due to unconnected and inaccessible pore space.

Drainage experiments require brine and CO_2 to be equilibrated under experimental conditions prior to injection to avoid drying out of the core sample (Perrin and Benson, 2010). Drainage (k_{rg}^d) is implemented by pumping CO_2 into the brine saturated sample until the irreducible water saturation is reached and maximum CO_2 saturation (S_{max}) is measured.

Experiments can flow CO_2 through cores using either steady-state or unsteady-state methodology. Steady-state involves driving a fixed ratio of two phases at constant rate through the sample until constant saturation and differential pressure is reached along the length of the core and produced ratio equals the injection ratio (Müller, 2011). Unsteady-state involves the injection of single fluid phases during the drainage and imbibition stages of the experiment (Bachu, 2013). Comparisons of these two techniques have shown no differences for obtaining relative permeability data in CO_2–brine systems (Mathias et al., in press). Due to the flow and pressure stabilisation, and hence greater time consumption, required for the steady-state method (Müller, 2011) experimental studies have commonly used the unsteady-state technique.

The duration of drainage experiments are not regularly reported in experimental publications. Pentland et al. (2011b) give a range of 14–166 h; while Pentland et al. (2010) give a range of 23–182 h for a suite of experiments investigating the trapping of oil during water flooding. All flow rates that have been published fall in the range thought to be representative of fluid velocity near the injection well for a large storage project (Perrin and Benson, 2010).

Once brine has reached irreducible water saturation the imbibition cycle is instigated by flooding brine back through the sample until CO_2 relative permeability reaches zero and the trapped CO_2 saturation (S_t) can be obtained. We find no published numbers concerning the duration of the imbibition stage, though Shi et al. (2011a,b) show that the injection rates of the imbibition phase in relation to the drainage phase are of the order of 4–22% and describe brine breakthrough at the core outlet after just under half the equivalent volume of brine had been injected (Shi et al., 2011b).

S_{max} and S_t can be measured using techniques such as CT scanning (e.g. Shi et al., 2011a,b; Perrin and Benson, 2010), volume balance and thermal depressurisation of CO_2 (Pentland et al., 2011a) or numerical regression methods which utilise measured values of phase flow rate and pressure drop during core flooding (Bennion and Bachu, 2005). CT scanning is the most advanced method as it allows the drainage/imbibition front to be tracked. It can also be used to generate continuous two dimensional porosity and saturation maps which can help identify heterogeneity and non-uniform displacement (Akin and Kovscek, 1999). However, in some cases the brine used is doped with sodium iodide (NaI) in order to enhance the contrast on CT images (Shi et al., 2011a). This has a potentially negative effect on maximum CO_2 saturation as NaI increases brine salinity; leading to a reduction in CO_2 solubility and an increase in the capillary pressure of the CO_2 phase (Bennion and Bachu, 2008).

2.2. Experimental biases

Experiments have mainly focused on the primary target lithology for most storage projects: high permeability sandstones. Few typical caprock shale samples have been considered. Storage reservoir heterogeneity, such as cemented fractures and stratigraphic variability (Caruana and Dawe, 1996), is not characterised within these experiments (Huppler, 1970). The hope is that they represent some averaged behaviour, but the criteria that make for a good experimental sample are unlikely to correspond to a good sampling strategy for characterising reservoir heterogeneity. Consequently, up scaling the results to a real reservoir is problematic.

There are also potential issues with the experimental set-up and the running conditions that may produce systematic differences between laboratories and account for some of the spread in the data. For example inadequate equilibration of brine and CO_2 prior to the drainage stage of the experiment may instigate drying out of the core.

Experimental flow rate is a major control. High flow rates represent conditions proximal to the injection point and diminishing flow rates represent some distance from the point of injection (Perrin and Benson, 2010). High flow rates produce larger S_{max} values (Shi et al., 2011a,b). Low flow rate experiments, typical for the bulk of the reservoir, are more time consuming and expensive. Contemporary studies on oil–water systems (Chen and Wood, 2001) show that low flow rates create uneven pressure regimes across the core: leading to capillary pressure discontinuities, brine retention at the core outlet and S_{max} underestimation. This effect can be overcome by dramatically increasing the flow rate and performing a 'bump flood' (Naylor et al., 2000) or by utilising a porous plate technique, which involves the emplacement of a hydrophilic semi-permeable disc at the outlet end of the core sample (Pentland et al., 2011b).

Samples from different depths within a single well have been noted to produce different values for porosity and permeability data (Crotti et al., 1998). Analyses of samples from different wells within the same formation under identical experimental conditions, by Bachu (2013), Bennion and Bachu (2008) and Shell (2011), highlight the potential range in heterogeneity demonstrated by a single reservoir formation (see Section 3.1.3).

Despite potential biases in experimental techniques and the small number of published values, the presentation of $k_r^{CO_2}$, S_{max} and S_t remains the best evidence base available for quantifying the storage security of geological CO_2 storage operations.

3. Analysis of publicly available data

3.1. Experimental results

Here we reanalyse available published end point saturation values in order to inform injectivity and storage security. Relatively few studies of CO_2–brine relative permeability and residual saturation have been published in the academic literature.

The most comprehensive data is from stand-alone experimental studies (Bennion and Bachu, 2008; Shi et al., 2011a,b). Since such data has been needed for some time to condition reservoir modelling studies, a variety of empirically conditioned estimates of end point saturations also exist. We include such data in this study for comparison. For example, Juanes et al. (2006) directly use the results of Oak's (1990) low pressure nitrogen–brine system study of the Berea Sandstone for their CO_2–brine simulations.

3.1.1. Sandstones

The majority of measurements hail from high permeability reservoir sandstones (Table 1). All experimental measurements are carried out under supercritical CO_2 conditions and measured values of endpoint $k_r^{CO_2}$ are recorded at S_{max}.

Summary figures presenting CO_2 endpoint saturations (S_{max}, S_t) against endpoint relative permeability ($k_r^{CO_2}$) values are plotted in Fig. 2. Marginal histograms along each axis summarise parameter distributions.

S_{max} ranges between 0.31 and 0.85, with a relatively normal distribution. S_t values are grouped over a tighter range (0.10–0.52) and skewed towards lower saturation values. Endpoint $k_r^{CO_2}$ values have a relatively even distribution, mainly within a range of 0.06–0.61, though the two values from the Shell (2011) study have $k_r^{CO_2}$ values close to one.

The percentage of residually trapped CO_2 (R) is estimated using the ratio of S_t to S_{max}. R values for sandstones range between 12.8% and 91.6% and are skewed to higher values with over half of the thirty trapping ratios being greater than 60% (Fig. 3) and only three values below 40%.

S_{max} values applied in the simulation studies are biased towards the upper end of experimental values ($k_r^{CO_2} = 0.7 - 0.8$ and $S_{max} = 0.7$–0.8). Simulation values for S_t plot within the range demonstrated by experimental values. The bias of S_{max} towards higher values underestimates trapped CO_2 and therefore overestimates CO_2 mobility in simulations. Average simulation R is 39%, which is 22% lower than the experimental values. In part, this disparity is derived from suboptimal sourcing of data, for example Juanes et al. (2006) parameters are derived from experimental studies of a low pressure brine–nitrogen gas system which they admit may not be entirely appropriate to represent supercritical CO_2 systems. When formation specific data is not available, the simulations can be improved by using the parameter distributions compiled in this paper as a starting point.

3.1.2. Carbonates and shales

We present the same endpoint analysis for both carbonates and shales in Fig. 4. All the data is from the experimental studies of Bennion and Bachu (2006, 2007, 2008, 2010) which use samples from Alberta, Canada.

For the carbonates, the mean S_{max} is 0.48 which compares to a mean for the sandstones of 0.53. The two data points for shale are 0.362 and 0.395 and are lower than all but two of the sandstone and two of the carbonate values. The measurements of S_t on both lithologies are comparable with the measurements in the sandstones. All of the shale samples and all but three of the carbonate samples have low $k_r^{CO_2}$ values (<0.2). For comparison over half of the sandstone values are above 0.2. The histogram in Fig. 4 demonstrates a tighter clustering for this value in comparison to sandstones. This may hint that low values and tight ranges of $k_r^{CO_2}$ could be a general trend in carbonates; which is an interesting observation as one would probably expect a wider range of $k_r^{CO_2}$ due to the greater heterogeneity and complexity of carbonate pore space in comparison to sandstones.

The R values for the nine carbonate imbibition samples are plotted in Fig. 3. The values produce a relatively uniform distribution and lie within the range of values for sandstones. The mean value, 50%, is 11% less than that of sandstones. The increased complexity of carbonate pore structures, due to the rocks biogenic origin, and their higher chemical reactivity will likely produce more complicated trends in endpoint relative permeability and residual saturation values than for reservoir sandstones.

The R values for the two shale samples (71% and 89%) lie above the sandstone range. The poorly interconnected pores and fluid flow pathways in shale may make it difficult for brine to flush CO_2 from the rock during imbibition. Despite high R values, low porosity values show that there is little fluid capacity in the sample pore space and low absolute permeability values demonstrate the lack of pore connectivity and difficulty of fluid to flow through shale.

3.1.3. Covariances, replicate samples and environmental conditions

The presence of covariance between S_{max}, S_t and $k_r^{CO_2}$ is explored in Fig. 5. When the CO_2 saturation (S_{max}) of the pore network is high, many of the permeable pathways will be occupied by CO_2 which we interpret as explaining the high endpoint $k_r^{CO_2}$ (Fig. 5a). There is no evidence of a trend between S_{max} and S_t (Fig. 5c), though there is a corresponding reduction in the R with increasing S_{max} as high permeability pathways are easy to re-flood with brine (Fig. 5e). High R values are associated with high S_t (Fig. 5f), though it must be noted that the absolute volume of trapped CO_2 will be low for small values of S_{max}. This is discussed in greater detail in Section 4.2.

Where the vertical variable is R, dashed lines signify mean R values for sandstone, carbonate and simulated sandstone. Fig. 5f shows that the mean R for simulated sandstone lies below the $\pm 1\sigma$ range on the mean R for sandstone. Fig. 5a–c further illustrates the bias in the choice of parameterisations for the simulation based studies (represented by triangles) compared to measured data.

At least two samples have been subjected to imbibition experiments for each of the North Sea basin Captain Sandstone (Shell, 2011); and the Alberta basin Cardium, Viking, Ellerslie, Basal Cambrian, Deadwood and Nisku formations (Bachu, 2013; Bennion and Bachu, 2008, 2010). In all cases, bar the Deadwood Formation and some of the Basal Cambrian Formation, samples from different wells were subjected to the same temperature, pressure and salinity conditions (Table SM1).

The North Sea basin Captain Sandstone samples (Table 1: 10a and 10b) have identical porosities and high permeabilities with the first having double the value of the second sample. Values for $k_r^{CO_2}$ and S_{max} are also identical but the second sample has S_t value 75% that of the first sample. This difference is reflected in the R values of the two samples.

The Cardium Formation samples (1e and 1f) have similar porosity but the second sample had an absolute permeability sixty times the first. The second sample has lower values for both $k_r^{CO_2}$ and S_{max} leading to an R value four times greater than the first sample.

Table 1
Published experimental values for residual saturation trapping (R).

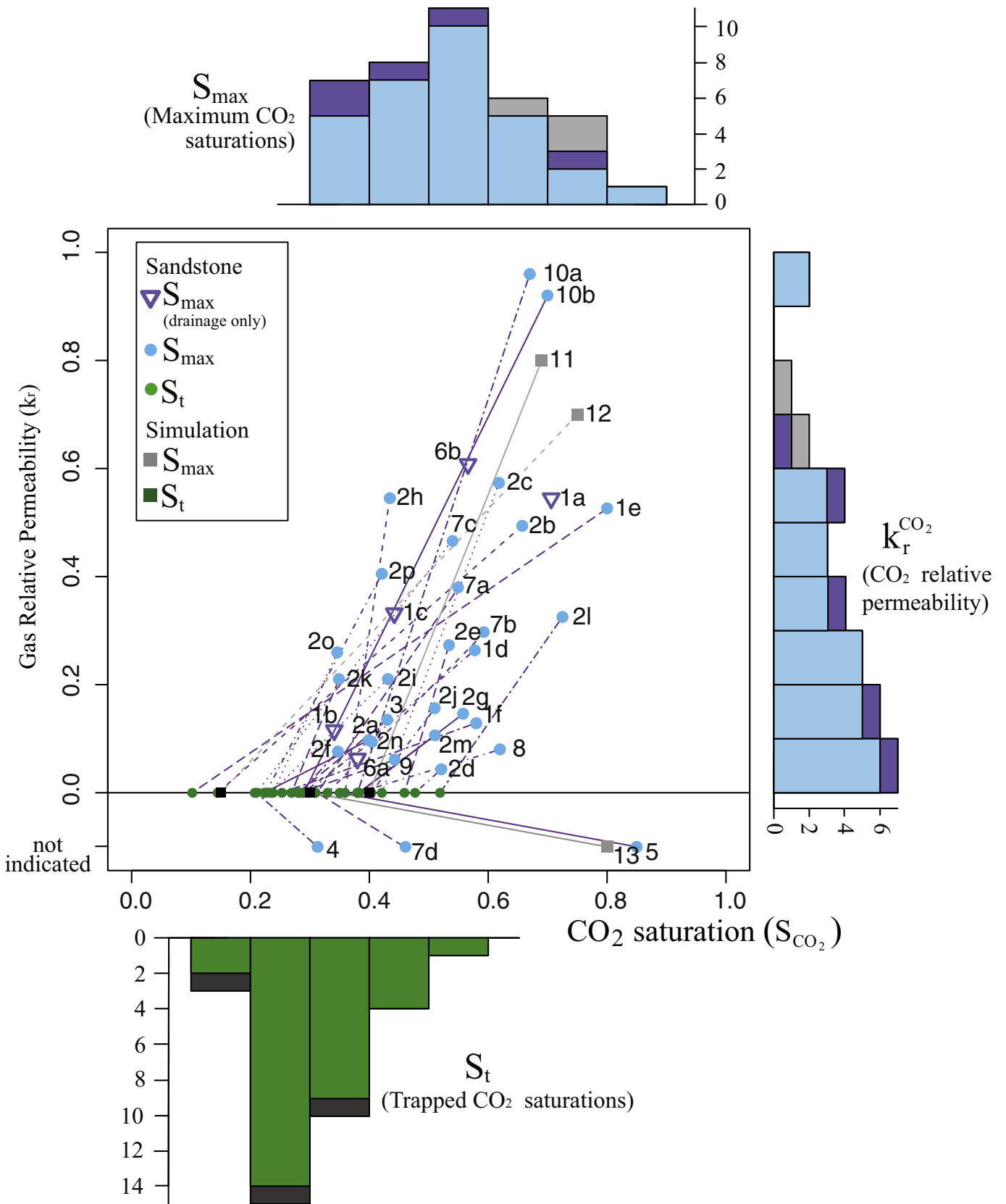| Lithology	Study	Location	Sample name	Mean Φ	k (mD)	$k_r^{CO_2}$	S_{max}	S_t	R (%)	Label
Sandstone	Bennion and Bachu (2008)	Alberta, Canada	Basal Cambrian Fm	11.7	0.081	0.5446	0.706	–	–	1a
			Ellerslie Fm	12.6	0.376	0.1156	0.341	–	–	1b
			Viking Fm #1	12.5	2.7	0.3319	0.442	–	–	1c
			Viking Fm #2	19.5	21.7	0.2638	0.577	0.297	51.5	1d
			Cardium Fm #1	15.3	0.356	0.5260	0.800	0.102	12.8	1e
			Cardium Fm #2	16.1	21.2	0.1290	0.580	0.253	43.6	1f
	Bachu (2013)	Alberta, Canada	Viking Fm #3	17.2	1.558	0.0973	0.399	0.223	55.9	2a
			Clearwater Fm	33.1	0.0164	0.4939	0.657	0.145	22.1	2b
			Ellerslie Fm #2	29	3.812	0.5735	0.618	0.421	68.1	2c
			Rock Creek Fm	14.5	65	0.0434	0.521	0.477	91.6	2d
			Halfway Fm	17.7	54.2	0.2733	0.534	0.459	86.0	2e
			Belloy	23.6	536.6	0.0762	0.347	0.283	81.6	2f
			Graminia Fm	31.6	133.9	0.1461	0.558	0.383	68.6	2g
			Gilwood Fm	11.5	0.749	0.5454	0.4345	0.3592	82.7	2h
			Basal Cambrian Fm #2	11.6	0.0057	0.2105	0.431	0.2339	54.3	2i
			Basal Cambrian Fm #3	11.9	252.5	0.1562	0.51	0.403	79.0	2j
			Basal Cambrian Fm #4	11.9	157.8	0.21	0.349	0.269	77.1	2k
			Basal Cambrian Fm #5	12.5	0.03	0.3255	0.725	0.519	71.6	2l
			Deadwood Fm #1	17.6	103.7	0.1062	0.5103	0.382	74.9	2m
			Deadwood Fm #2	16.2	69.1	0.0941	0.4041	0.2883	71.3	2n
			Deadwood Fm #3	19.3	137.9	0.2597	0.346	0.238	68.8	2o
			Granite Wash	14.8	70.1	0.405	0.4211	0.2256	53.6	2p
	Shi et al. (2011a)	Japan	Tako Sandstone	27	55.4	0.135	0.43	0.28	65.1	3
	Shi et al. (2011b)	OH, USA	Berea	18.7	330	–	0.313	0.21	67.1	4
	Pentland et al. (2011a,b)	OH, USA	Berea	22	446	–	0.85	0.35	41.2	5
	Perrin and Benson (2010)	OH, USA	Berea	20.3	430	0.063	0.38	–	–	6a
		Australia	Otway Basin	18.2	45	0.608	0.566	–	–	6b
	Krevor et al. (2012)	OH, USA	Berea	22.1	914	0.38	0.55	0.31	56.4	7a
		Australia	Paaratte	28.3	1.156	0.3	0.59	0.33	55.9	7b
		IL, USA	Mt. Simon	24.4	7.5	0.46	0.54	0.21	38.9	7c
		MS, USA	Tuscaloosa	23.6	220	–	0.46	0.31	67.4	7d
	Mackay et al., 2010	Elgin, Scotland	Clashach	–	–	0.08	0.62	0.38	61.3	8
		Lincolnshire, England	Sherwood	–	–	0.061	0.443	0.283	63.9	9
	Shell (2011)	Goldeneye Field, North Sea	Captain #1	26.3	2,048	0.96	0.67	0.38	56.7	10a
			Captain #2	26.9	1,025	0.92	0.7	0.29	41.4	10b
Simulation	Juanes et al. (2006)	OH, USA	Berea	20	100	0.8	0.690	0.4	58.0	11
	Sifuentes et al. (2009)	TX, USA	Frio Fm	25	100	0.7	0.75	0.15	20.0	12
	Yang (2008)	Browse Basin, Australia	Carbine	10	304	–	0.8	0.3	37.5	13
Shale	Bennion and Bachu (2008)	Alberta, Canada	Calmar Fm	3.9	2.94E−06	0.1871	0.362	0.256	70.7	14a
			Colorado Gp	4.4	7.88E−05	0.0148	0.395	0.349	88.4	14b
Carbonate	Bennion and Bachu (2008)		Cooking Lake Fm	9.9	65.3	0.0685	0.524	–	–	15a
			Nisku Fm #1	9.7	45.9	0.1768	0.670	–	–	15b
			Nisku Fm #2	11.4	21	0.0999	0.508	0.218	42.9	15c
			Wabamun #1	7.9	0.018	0.5289	0.405	–	–	15d
			Wabamun #2	14.8	67	0.1883	0.431	–	–	15e
	Bennion and Bachu, 2010	Alberta, Canada	Wabamun #3	15.4	54.3	0.1015	0.148	0.045	30.4	16a
			Nisku Fm #3	10.9	74.4	0.1078	0.603	0.207	34.3	16b
			Grosmont	11.8	153.9	0.1101	0.48	0.356	74.2	16c
			Morinville Leduc	11.6	371.9	0.0746	0.47	0.131	27.9	16d
			Redwater Leduc	16.8	353.6	0.0476	0.335	0.208	62.1	16e
			Cooking Lake #2	16.7	4.9	0.094	0.4037	0.268	66.4	16f
			Slave Point	9.9	0.217	0.5037	0.454	0.256	56.4	16g
			Winnipegosis	14.8	3.1	0.6117	0.7892	0.4149	52.6	16h

Fig. 2. Scatter plot of published relative permeability data for sandstones. Data point number identifiers correlate with the values presented in Table 1. Purple triangles correspond to experimental measurements where only S_{max} was measured. Blue S_{max} circles indicate experiments where S_t was measured (green circles). Empirically conditioned values are represented by light (S_{max}) and dark green (S_t) squares. In all cases corresponding data points are connected by dashed lines. Studies which did not provide values for $k_r^{CO_2}$, either because it was not documented (Yang, 2008; Shi et al., 2011b) or because the experimental set up did not allow for its measurement (Pentland et al., 2011b), are plotted below 0. The x axis shows marginal histograms for S_{max} (upper) and S_t (lower) and the y axis shows a histogram of $k_r^{CO_2}$ at S_{max}.
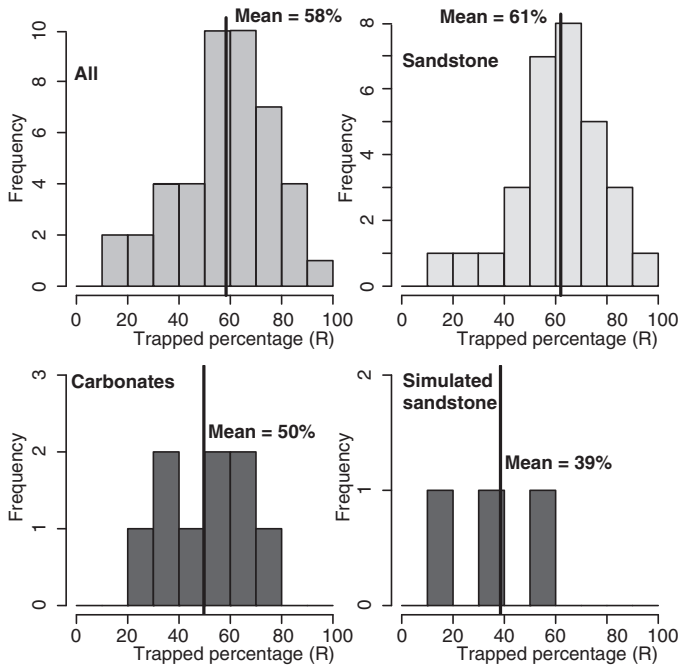
Fig. 3. Histograms of CO_2 trapping ratio ($R = S_t/S_{max}$). Values included are from the complete imbibition experiments shown in Figs. 3 and 5 (i.e. values connected by dashed lines).

Despite varying $k_r^{CO_2}$ and S_{max} values the R value of two Viking Fm samples are within 4.4% (1d and 2a). Two of the four Basal Cambrian Fm samples (2i–2l) were exposed to the same experimental conditions (2i and 2l). The two experimentally identical samples have an R value difference of 17%, whilst three experimentally different samples (2j–2l) are within 7.4%. The three experimentally different Deadwood Fm samples (2m–2o) have R values within 6.1%. The R value similarity in the experimentally different examples indicates that R for a single core sample may potentially provide a good approximation for reservoir-wide residual saturation trapping.

The carbonate Nisku Formation samples (15c and 16b) have similar mean porosity and $k_r^{CO_2}$. The S_{max} value of 16b is 0.1 greater and the absolute permeability 3.5 greater. Easier access to connected fluid flow pathways during imbibition may be reason that 16b has an R value 9% less than 15c.

The Berea Sandstone has been analysed in four separate studies (Table 1: 4–7). For the three imbibition studies there is a wide range of R (41.2–67.1%). It is hard to compare the effects of different parameters on the R values due to the large differences in absolute permeability, S_{max} and experimental conditions. Endpoint $k_r^{CO_2}$ data is available for two studies, with the value for the drainage only experiment of Perrin and Benson (2010) 1/16 that of Krevor et al. (2012). Perrin and Benson (2010) investigated rock heterogeneity effects sub-parallel to the flow direction. They note that the higher porosity layer within the sample was disconnected from the inlet face of the core, leading to a relatively low $k_r^{CO_2}$ value. Despite the differences in experimental conditions (Table SM1) this may give an indication of the vertical to horizontal permeability ratio for this sandstone.

4. Discussion

The published CO_2 saturation values reviewed in this paper allow us to start making evidence based statements for injectivity, incomplete saturation, CO_2 gas phase residual trapping and the insurability of CO_2 geological storage sites.

4.1. Statements on injectivity

Injectivity describes the rate with which CO_2 can be injected into a geological storage reservoir given the geology and some downhole fluid pressure differential between borehole and storage formation. The downhole pressure is also limited by safety considerations and running costs inherent in pressuring the CO_2. Consequently, the well design and number of wells that are required to achieve a target injection rate are directly dependent upon the injectivity.

Injectivity is proportional to the relative permeability through Darcy's Law. The measurements of endpoint relative permeability in reservoir sandstones (Table 1) for supercritical CO_2 vary over an order of magnitude (0.06–0.6). In the worst case, this implies an order of magnitude uncertainty in well density due to endpoint relative permeability uncertainty. One possible strategy for reducing uncertainty is the weak scaling of endpoint relative permeability with maximum saturation (Fig. 5a), a measurement which is easier and cheaper to make. Relative permeability values do not scale with trapped saturation (Fig. 5b). Endpoint relative permeability is measured at the maximum saturation and we have already shown the maximum and trapped saturations to be relatively independent (Fig. 5c).

It is therefore important to measure the relative permeability of CO_2 within a sample of reservoir rock to de-risk uncertainty in achievable injection rates and for design of the injection facility. However, scale up issues must be kept in mind. Though lab experiments can simulate field scale injection rates a 10–100 mm core sample cannot accurately represent reservoir thicknesses.

4.2. Incomplete saturation and stability of the plume front

The data explored above quantifies the security provided by residual saturation for end point saturations. Here we explore how the percentage trapping varies when the maximum saturation of the CO_2 injected into the rock is not reached in order to see whether the proportion of residually trapped CO_2 calculated using the endpoint saturations is likely to be an optimistic or conservative estimate.

The Land model (Land, 1968) can be used to estimate the incomplete trapped saturation (S_t^*) that will be realised during the imbibition of CO_2 from a rock when the saturation of CO_2 attained during the drainage of the water phase (S_{max}^*) did not reach it maximum saturation (S_{max}). In other words, the relative permeability of the water phase had not gone to zero before imbibition started.

The Land model for incomplete saturation of the CO_2 phase is illustrated in Fig. 6. When water flood occurs at some point before maximum gas saturation is reached (S_{max}^*) then the resulting incomplete trapped saturation (S_t^*) can be calculated according to Land by,

$$S_t^* = \frac{S_{max}^*}{1 + C S_{max}^*} \tag{1}$$

where the constant C is the Land trapping coefficient, which is a function of S_t and S_{max} which are ideally determined experimentally,

$$C = \frac{1}{S_t} - \frac{1}{S_{max}} \tag{2}$$

In the case of incomplete saturation (S_{max}^*) during CO_2 flooding the change in residual trapping efficiency (R) can be calculated by rewriting S_{max}^* as S_{max} minus some shift which describes how far we are from S_{max}^*;

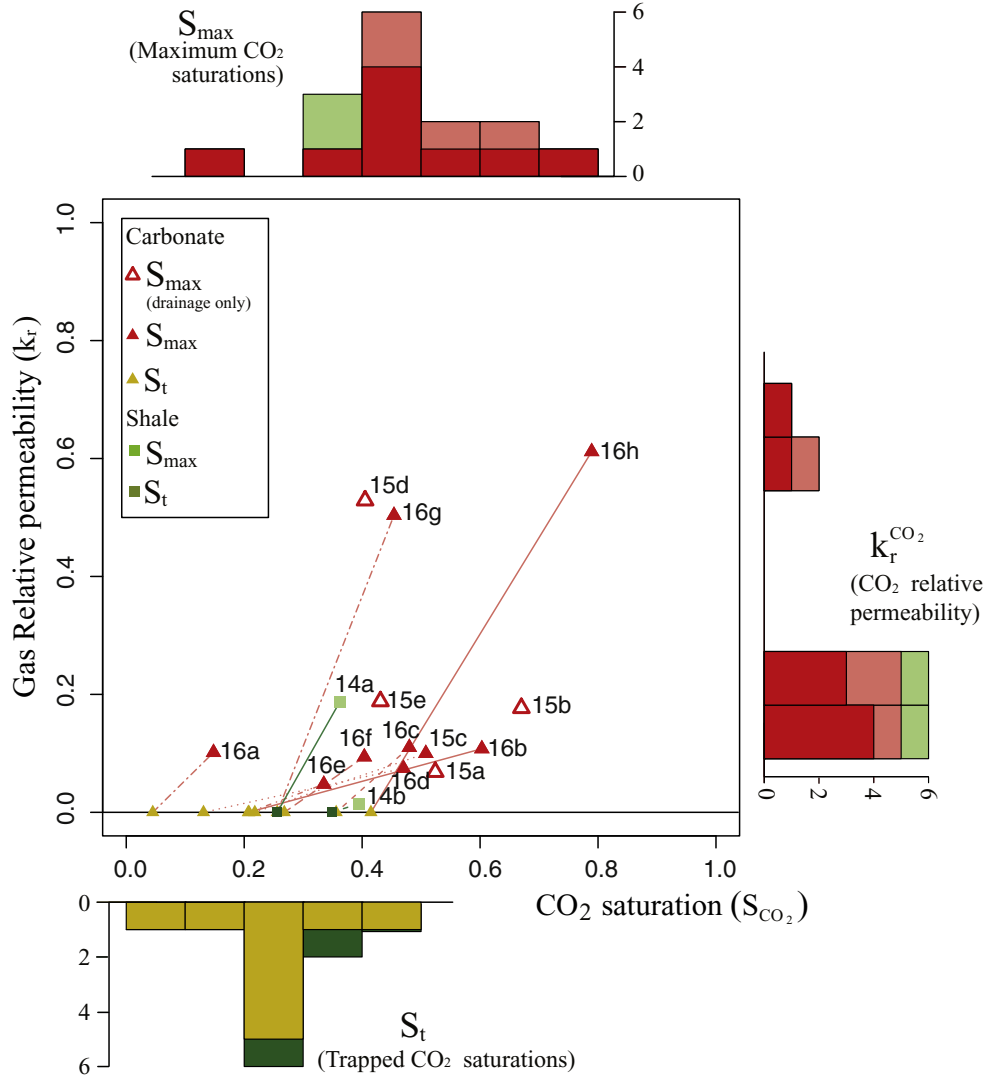$$S_{max}^* = S_{max} - \delta \tag{3}$$

Fig. 4. Plot of published relative permeability data for carbonates and shales. The number identifiers refer to data in Table 1. The open, pink triangles represent drainage only experiments for carbonate. The red and gold triangles correspond to S_{max} and S_t s results of the only combined drainage–imbibition experiment for a carbonate. Shale results are demonstrated by light and dark green squares for S_{max} and S_t respectively.

and substitute this into the Land equation rearranged for the percentage of residually trapped CO_2 (R^*);

$$R^* = \frac{S_t^*}{S_{max}^*} = \frac{1}{1 + CS_{max}^*} = \frac{1}{1 + C(S_{max} - \delta)}$$

$$= \frac{1}{1 + (S_{max} - \delta)/S_t - (S_{max} - \delta)/S_{max}}$$

$$= \frac{1}{(S_{max}/S_t) - (\delta/S_t) + (\delta/S_{max})} = \frac{1}{(S_{max}/S_t) - \delta C} \qquad (4)$$

where δ can take any value in the range 0 to S_{max}. In the limit $\delta = 0$, where $S_{max}^* = S_{max}$, we recover the original trapped percentage of CO_2, i.e. $R^* = R = S_t/S_{max}$.

This implies that at low levels of CO_2 saturation, $\delta \rightarrow S_{max}$ and the residual trapping efficiency increases, i.e. $R^* \rightarrow 1$. A further implication is that the plume front is stabilised by residual saturation trapping. This greater level of storage security is tempered by the fact that the gas saturation is lower than the maximum so a smaller fraction of injected CO_2 will become permanently stored per unit of rock.

In summary, the use of end point saturations in the estimation of trapping ratios (R) is conservative with respect to incomplete saturation.

4.3. The need for CO_2 gas phase residual trapping

Relative permeability experiments performed to inform on CO_2 storage have understandably focussed on behaviour under target storage conditions, which are assumed to be supercritical CO_2. Experimental data is also needed for CO_2 in the gas phase. Some demonstration projects are looking to store CO_2 in depleted gas fields in a gaseous state (Total, 2007).

Gas phase experiments are important to better understand the effects of residual trapping in the overburden should injected CO_2 escape from the storage reservoir. As migrating supercritical CO_2 ascends it will transition into gas phase CO_2 via one of the two main processes depending on local surface temperature (Doughty and Myer, 2009). For higher surface temperatures ($\sim$>10 °C) CO_2 has a smooth transition from super critical to gas phase. For lower surface temperatures ($\sim$<10 °C) ascending CO_2 will cross the CO_2 liquid-gas saturation line. Here CO_2 properties change abruptly and three phase flow dominates as CO_2 makes the transition from liquid
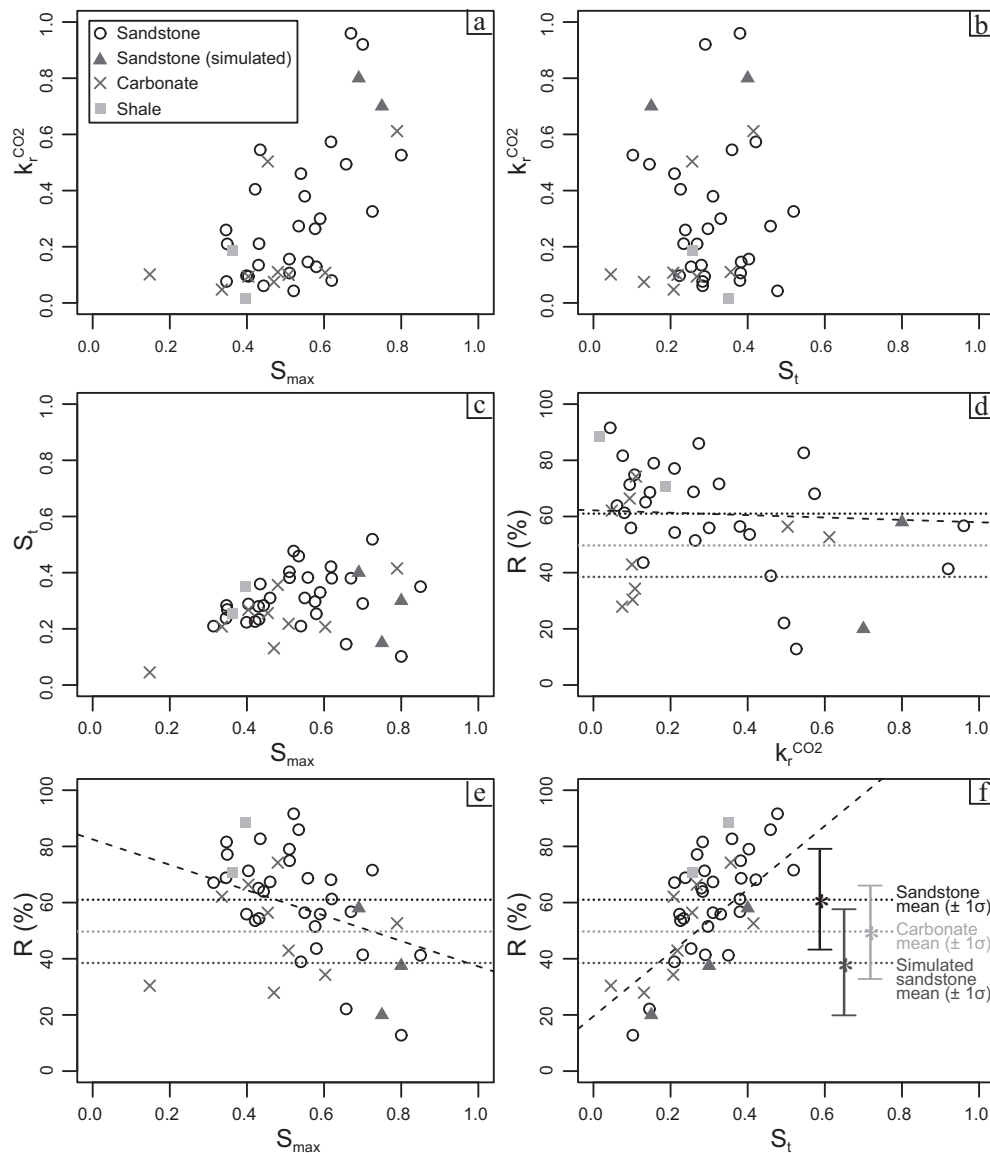
Fig. 5. Plots of endpoint relative permeability, endpoint saturation and trapping ratio. Studies with no measured or calculated value for $k_r^{CO_2}$ are excluded from plots (a) and (b). The trend line shown in (f) is solely for guidance as the data generally displays a broad scatter over a wide range of values.

to gas phase (Doughty and Myer, 2009). The depth of the liquid–gas saturation line is site specific as it depends on local temperature and pressure regimes. Given saturation line temperature and pressure ranges it is typically situated at a depth of no more than 600 m.

The experiments that have been performed (Table 1) describe the residual saturation behaviour for supercritical phase CO_2 at storage reservoir temperature and pressure conditions. To gain a real appreciation of trapping effects on gas phase CO_2 experiments need to be conducted using appropriate parameters. We should not expect the results detailed in Table 1 to translate directly to the gas phase. Gas phase CO_2 has the viscosity of supercritical CO_2 but has a lesser density, giving it the potential of comparatively rapid vertical migration. The relatively shallow depths that gas phase CO_2 dominate will typically have less saline brine, lower temperature and pressure conditions, and possibly higher porosity due to less rock compaction and secondary mineralisation. For investigation of CO_2 that has migrated into the shallow subsurface experimentation using loosely or unlithified sediments would be extremely useful to determine the fraction of a pre-determined mass of CO_2 that can reach the surface.

4.4. Use of relative permeability data in reservoir simulations

Mathematical methods have been used to estimate endpoint relative permeability and saturations for use in reservoir simulations and other mathematical models of CO_2 storage. These estimates are either semi-empirically conditioned (Juanes et al., 2006), values from historic oil field studies (Flett et al., 2004), calculated from correlations (Kumar et al., 2005) or the source of their value is not discussed (Gasda et al., 2011; Wei and Saaf, 2009; Nghiem et al., 2009). In this section we compare mathematically determined values of three semi-empirically conditioned models with the experimental values in order to assess whether the results of simulations based on mathematically determined values are likely to be biased.

Values of S_{max} and $k_r^{CO_2}$ used in the simulations are biased towards higher values (Fig. 5a), suggesting that potential injectivities may be overestimated in simulations, which impacts upon the required well density, well design and injection strategy. The values of S_{max} in the simulations are typically large in comparison to the experimental data whilst the values for S_t are generally in line
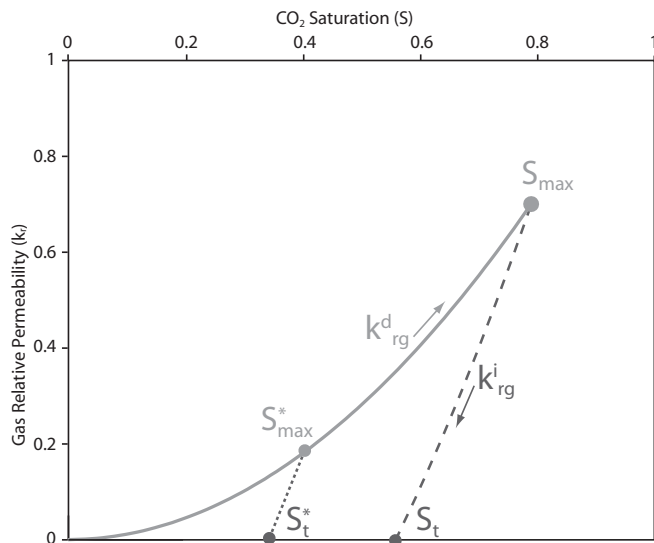
Fig. 6. Land residual gas trapping model demonstrating imbibition curve for incomplete CO_2 saturation. Drainage curve is shown in light grey and imbibition curves for S_t (long dashed line) and S_t^* (short dashed line) are shown in dark grey.

with the range represented by the experimental values. The end result is an underestimation of *R* in comparison to experimental values (Fig. 3). This means that the fraction of mobile CO_2 will be overestimated in comparison to experimental data, leading to the predicted migration of injected CO_2 exceeding natural migration.

Direct comparison between semi-empirically derived values and individual experimental results are hard as there has been little cross-over in the reservoirs being investigated. Of the three models only one can be directly compared with three of the experimental residual saturation values as they all investigate the same lithology. The CO_2 saturation values calculated by Juanes et al. (2006) for the Berea Sandstone sit comfortably with the values from the experimental results of Pentland et al. (2011b), Shi et al. (2011a,b) and Krevor et al. (2012). This is perhaps unsurprising as the CO_2 relative permeability is based on physical experiments. The S_{max} and S_t values of Juanes et al. (2006) sit close to those of Pentland et al. (2011b), however widely differing values of intrinsic permeability and temperature and missing information about salinity from Juanes et al. (2006) and $k_r^{CO_2}$ from Pentland et al. (2011b) make a closer comparison difficult.

4.5. Insurability of storage sites

In order for a geological storage project to proceed it will require some kind of storage permit from local government, which likely will only be granted if the project operator can secure some kind of financial security mechanism (Haszeldine, 2011). There are several types of financial security available (DECC, 2009; EC, 2011); but it is unclear which is the best option for cost or financial security as geological CO_2 storage is an emerging market with no direct analogy. Under the European Union Emission Trading Scheme (EU-ETS) all financial security mechanisms require large balance-sheet sums to be set aside by the operator to cover emissions liability in the event of leakage. For multi-million tonnes CO_2 storage projects covering 100% of injected CO_2 under this stipulation would require operators to ring-fence unfeasible sums running into 10's of billions of Euros for many decades (Haszeldine, 2011).

Experimental residual saturation trapping information can be used to quantify security and help reduce the financial exposure faced by geological storage site operators. The compiled data presented in this paper show an *R* range of 13–92% for sandstone with

a mean value of 61%. If we take these numbers as representative of a typical sandstone storage reservoir then it can be said that of the total volume of CO_2 injected only 39% can possibly migrate out of the storage reservoir in the event of primary seal failure. This is an important observation as it allows us to move beyond the regulatory assumption that all injected CO_2 can escape should the storage reservoir become compromised.

5. Conclusion

The values of CO_2 residual saturation presented in this review show consensus that a significant fraction of CO_2 will be immobilised within the storage reservoir. Thirty sandstone samples have a trapping ratio range of 13–92% and a mean value of 61%. In the event of leakage from the reservoir this residually trapped fraction of the injected CO_2 plume will remain in place.

Experiments have mainly focused on the drainage phase due to the comparatively complex and time consuming nature of the imbibition phase. The available published values show that for a wide range of maximum CO_2 saturation values, trapped CO_2 saturation values are tightly constrained. CO_2 trapping ratios are positively related to trapped saturations, inversely related to maximum saturations and show no strong relation with endpoint relative permeability. More data is needed but these trends may hint at the ability to predict trapping ratios from maximum CO_2 saturations. Using maximum saturation measurements from multidirectional core samples may provide a time effective method for representing CO_2 residual trapping heterogeneity in reservoir simulations.

In order to better parameterise simulation studies and increase confidence in storage security further experimental work is required. Focus should naturally be on sites which have been selected for demonstration or industrial scale projects so that monitoring of the CO_2 plume can be used to check the accuracy of experimental results. Multiple samples from single rock units (to give a range of values) and repeated experiments on single samples (to test effects of key parameters on saturation values) would further our understanding of residual trapping and provide greater confidence limits on the range of values presented in this paper.

References

Akin, S., Kovscek, A.R., 1999. Imbibition Studies of Low-Permeability Porous Media. In: SPE Western Regional Meeting, Anchorage, Alaska, 26–27 May, SPE 54590.

Anand, V., Freedman, R., Crary, S., Minh, C.C., Terry, R.L., 2010. Predicting effective permeability to oil in sandstone and carbonate reservoirs from well logging data. In: SPE Annual Technical Conference and Exhibition, 19–22 September 2010, Florence, Italy, SPE 134011.

Bachu, S., 2013. Drainage and imbibition of CO_2/brine relative permeability curves at in situ conditions for sandstone formations in western Canada. In: Proceedings of the 11th International Conference on Greenhouse Gas Control Technologies, November 18–22, 2012, Kyoto, Japan, Elsevier, Energy Procedia, v. 37, pp. 4428–4436.

Baines, S.J., Worden, R.H., 2004. The long term fate of CO_2 in the subsurface: natural analogues for CO_2 storage. In: Baines, S., Worden, R.H. (Eds.), Geological Storage of Carbon Dioxide, vol. 233. Geological Society Special Publications, London, pp. 59–85.

Bennion, D.B., Bachu, S., 2005. Relative permeability characteristics for supercritical CO_2 displacing water in a variety of potential sequestration zones in the Western Canada Sedimentary Basin. In: SPE Paper No. 95547.

Bennion, D.B., Bachu, S., 2006. Supercritical CO_2 and H_2S – Brine drainage and imbibition relative permeability relationships for intercrystalline sandstone and

carbonate formations. In: SPE Europec/EAGE Annual Conference and Exhibition, Vienna, Austria, Society of Petroleum Engineers.

Bennion, D.B., Bachu, S., 2007. Permeability and relative permeability measurements at reservoir conditions for CO_2–water systems in ultra low permeability confining caprocks. In: EUROPEC/EAGE Conference and Exhibition. Society of Petroleum Engineers, London, U.K..

Bennion, D.B., Bachu, S., 2008. Drainage and imbibition relative permeability relationships for supercritical CO_2/brine and H_2S/brine systems in intergranular sandstone, carbonate, shale, and anhydrite rocks. SPE Reservoir Evaluation and Engineering 11, 487–496.

Bennion, D.B., Bachu, S., 2010. Drainage and imbibition relative permeability curves at reservoir conditions for carbonate formations. In: SPE Paper 134028; SPE Annual Technical Conference and Exhibition, 19–22 September 2010, Florence, Italy.

Burnside, N.M., Shipton, Z.K., Dockrill, B., Ellam, R.M., 2013. Man-made versus natural CO_2 leakage: a 400 k.y. history of an analogue for engineered geological storage of CO_2. Geology 41, 471–474.

Caruana, A., Dawe, R.A., 1996. Flow behaviour in the presence of wettability heterogeneities. Transport in Porous Media 25, 217–233.

Chen, A.L., Wood, A.C., 2001. Rate effects on water–oil relative permeability. In: Proceedings of the International Symposium of the Society of Core Analysts, Volume Paper SCA 2001-19, 17–19 September, 2001, Edinburgh, Scotland.

Crotti, M.A., Inlab, S.A., Rosbaco, J.A., 1998. Relative permeability curves: the influence of flow direction and heterogeneities. Dependence of end point saturations on displacement mechanisms. In: SPE/DOE Improved Oil Recovery Symposium, Tulsa, Oklahoma, SPE 39657.

Department of Energy and Climate Change (DECC), 2009. A Consultation on the Proposed Offshore Carbon Dioxide Licensing Regime, URN 09D/753., pp. 29.

Doughty, C., Myer, L.R., 2009. Scoping calculations on leakage of CO_2, in geologic storage: the impact of overburden permeability, phase trapping, and dissolution. In: McPherson, B.J., Sundquist, E.T. (Eds.), Carbon Sequestration and its Role in the Global Carbon Cycle, Geophysical Monograph Series 183. , pp. 217–237.

European Commission, 2011. Guidance Document 4: Article 19 Financial Security and Article 20 Financial Contribution: Implementation of Directive 2009/31/EC on the Geological Storage of Carbon Dioxide.

Fetter, C.W., 1993. Contaminant Hydrogeology, 2nd Addition. Pretence-Hall International (UK) Limited, London.

Flett, M., Gurton, R., Taggart, I., 2004. The function of gas–water relative permeability hysteresis in the sequestration of carbon dioxide in saline formations. In: SPE Asia Pacific Oil and Gas Conference and Exhibition, Perth, Australia, Society of Petroleum Engineers.

Gasda, S.E., Nordbotten, J.M., Celia, M.A., 2011. The impact of local-scale processes on large-scale CO_2 migration and immobilization. Energy Procedia 4, 3896–3903.

Haszeldine, R.S., 2011. Geological factors in framing legislation to enable and regulate storage of carbon dioxide deep in the ground. In: Havercroft, I., Macrory, R., Stewart, R.B. (Eds.), Carbon Capture and Storage: Emerging Legal and Regulatory Issues. Hart Publishing, Oxford, pp. 7–23.

Huppler, J.D., 1970. Numerical investigation of the effects of core heterogeneities on waterflood relative permeabilities. SPE Journal 10, 381–392.

IPCC, 2005. IPCC Special Report on Carbon Dioxide Capture and Storage. Cambridge University Press, Cambridge.

Juanes, R., Spiteri, E.J., Orr Jr., F.M., Blunt, M.J., 2006. Impact of relative permeability hysteresis on geological CO_2 storage. Water Resource Research 42.

Krevor, S.C.M., Pini, R., Zuo, L., Benson, S.M., 2012. Relative permeability and trapping of CO_2 and water in sandstone rocks at reservoir conditions. Water Resource Research 48, W02532, http://dx.doi.org/10.1029/2011WR010859.

Kumar, A., Ozah, R., Noh, M., Pope, G.A., Bryant, S., Sepehrnoori, K., Lake, L.W., 2005. Reservoir simulation of CO_2 storage in deep saline aquifers. SPE Journal 10, 336–348.

Land, C.S., 1968. Calculation of imbibition relative permeability for two and three-phase flow from rock properties. SPE Journal 8 (2), 149–156.

Mackay, E., Pickup, G., Olden, P., 2010. Rock mechanics, geochemistry and aquifer fluid flow. In: CASSEM Conference, 4th October 2010, Edinburgh.

Mathias, S., Gluyas, J., Gonzalez, G., Bryant, S., Wilson, D., in press. On relative permeability data uncertainty and CO_2 injectivity estimation for brine aquifers. International Journal of Greenhouse Gas Control.

Müller, N., 2011. Supercritical CO_2–brine relative permeability experiments in reservoir rocks—literature review and recommendations. Transport in Porous Media 87 (2), 367–383.

Naylor, P., Fishlock, T.P., Mogford, D.J., Smith, R.A., 2000. Relative permeability measurements for post-waterflood depressurisation of the miller field, North Sea. In: Annual Technology Conference and Exhibition, Dallas, Texas, SPE 63148.

Nghiem, L., Yang, C., Shrivastava, V., Kohse, B., Hassam, M., Card, C., 2009. Risk mitigation through the optimization of residual gas and solubility trapping for CO_2 storage in saline aquifers. Energy Procedia 1, 3015–3022.

Oak, M.J., Baker, L.E., Thomas, D.C., 1990. Three-phase relative permeability of Berea sandstone. Journal of Petroleum Technology, Transactions, AIME 289, 1054–1061.

Pentland, C.H., Tanino, Y., Iglauer, S., Blunt, M.J., 2010. Capillary trapping in water-wet sandstones: core flooding experiments and pore-network modelling. In: SPE Annual Technical Conference and Exhibition, 19–22 September 2010, Florence, Italy.

Pentland, C.H., El-Maghraby, R., Georgiadis, A., Iglauer, S., Blunt, M.J., 2011a. Immiscible displacements and capillary trapping in CO_2 storage. Energy Procedia 4, 4969–4976.

Pentland, C.H., El-Maghraby, R., Iglauer, S., Blunt, M.J., 2011b. Measurements of the capillary trapping of super-critical carbon dioxide in Berea sandstone. Geophysical Research Letters 38 (6), L06401.

Perrin, J.-C., Benson, S.M., 2010. An experimental study on the influence of sub-core scale heterogeneities on CO_2 distribution in reservoir rocks. Transport in Porous Media 82 (1), 93–109.

Pickup, G.E., Jin, M., Olden, P., Mackay, E., Todd, A.C., Ford, J.R., Lawrence, D., Monaghan, A., Naylor, M., Haszeldine, R.S., Smith, M., 2010. Geological storage of CO_2: site appraisal and modelling. In: CASSEM report.

Saadatpoor, E., Bryant, S., Sepehrnoori, K., 2010. New trapping mechanism in carbon sequestration. Transport in Porous Media 82, 3–17.

Shell, 2011. UK Carbon Capture and Storage Demonstration Competition. UKCCS-KT-S7.19-Shell-002, SCAL Report. ScottishPower CCS Consortium, pp. 59.

Shi, J.-Q., Xue, Z., Durucan, S., 2011a. Supercritical CO_2 core flooding and imbibition in Berea sandstone—CT imaging and numerical simulation. Energy Procedia 4, 5001–5008.

Shi, J.-Q., Xue, Z., Durucan, S., 2011b. Supercritical CO_2 core flooding and imbibition in Tako sandstone—influence of sub-core scale heterogeneity. International Journal of Greenhouse Gas Control 5 (1), 75–87.

Sifuentes, W.F., Giddins, M.A., Blunt, M.J., 2009. Modeling CO_2 Storage in Aquifers: Assessing the Key Contributors to Uncertainty. Society of Petroleum Engineers, Offshore Europe, Aberdeen, UK.

Spiteri, E., Juanes, R., Blunt, M.J., Orr, F., 2008. A new model of trapping and relative permeability hysteresis for all wettability characteristics. SPE Journal 13, 277–288.

Total, S.A., 2007. Project Information Dossier: Lacq Basin CO_2 Capture and Geological Storage Pilot Project.

Wei, L., Saaf, F., 2009. Estimate CO_2 storage capacity of the Johansen formation: numerical investigations beyond the benchmarking exercise. Computational Geosciences 13, 451–467.

Wilkinson, M., Haszeldine, R.S., Fallick, A.E., Odling, N., Stoker, S.J., Gatliff, R.W., 2009. CO_2–mineral reaction in a natural analogue for CO_2 storage—implications for modeling. Journal of Sedimentary Research 79, 486–494.

Yang, Q., 2008. Dynamic modelling of CO_2 injection in a closed saline aquifer in the Browse Basin, Western Australia. In: SPE Asia Pacific Oil and Gas Conference and Exhibition, 20–22 October 2008, Perth, Australia, Society of Petroleum Engineers.